February 14, 2023
Volume 57
Number 6
pubs.acs.org/est

Environmental Science & Technology

ACS Publications
Most Trusted. Most Cited. Most Read.

www.acs.org

Environmental Science & Technology

pubs.acs.org/est

Article

"Urban Respiration" Revealed by Atmospheric O_2 Measurements in an Industrial Metropolis

Xiaoyue Liu, Jianping Huang,* Li Wang, Xinbo Lian, Changyu Li, Lei Ding, Yun Wei, Siyu Chen, Yongqi Wang, Shixue Li, and Jinsen Shi

Cite This: *Environ. Sci. Technol.* 2023, 57, 2286−2296

Read Online

ACCESS | Metrics & More | Article Recommendations | Supporting Information

ABSTRACT: Urban regions, which "inhale" O_2 from the air and "exhale" CO_2 and atmospheric pollutants, including harmful gases and fine particles, are the largest sinks of atmospheric O_2, yet long-term O_2 measurements in urban regions are currently lacking. In this study, we report continuous measurements of atmospheric O_2 in downtown Lanzhou, an industrial metropolis in northwestern China. We found declines in atmospheric O_2 associated with deteriorated air quality and robust anticorrelations between O_2 and gaseous oxides. By combining O_2 and pollutants measurements with a Lagrangian atmospheric transport model, we quantitatively break down "urban respiration" (ΔO_{2URB}) into human respiration (ΔO_{2RES}) and fossil fuel combustion (ΔO_{2FF}). We found increased ΔO_{2FF} contribution (from 66.92% to 72.50%) and decreased ΔO_{2RES} contribution (from 33.08 to 27.50%) as O_2 declines and pollutants accumulate. Further attribution of ΔO_{2FF} reveals intracity transport of atmospheric pollutants from industrial sectors and suggests transportation sectors as the major O_2 sink in downtown Lanzhou. The varying relationships between O_2 and pollutants under different conditions unfold the dynamics of urban respiration and provide insights into the O_2 and energy consumption, pollutant emission, and intracity atmospheric transport processes.

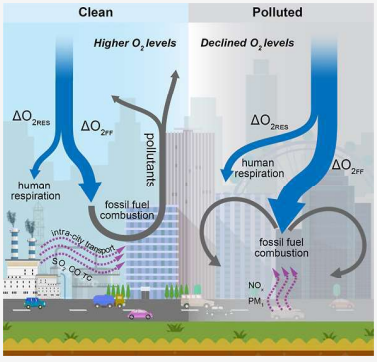

KEYWORDS: *urban O_2 measurements, air pollution, urban habitability, anthropogenic impact, vehicle pollutants*

INTRODUCTION

Urban regions, with their large and dense populations, only account for 2% of global lands, but are home to more than 56% of the global population[1] and responsible for 70% of global fossil-fuel combustion.[2] In recent decades, as growing population streams into cities, urban regions have faced serious challenges regarding climate change adaptation and mitigation. Rapid urban expansion and the related land-use change have left a series of urban environmental issues including record-breaking urban heatwaves,[3] extreme floods and droughts that overwhelm the undermaintained public infrastructures,[4] rising levels of air pollution,[5−7] and the emerging disturbed O_2 balance in urban regions.[8]

As a necessity for the survival of almost all living organisms on Earth, atmospheric oxygen (O_2) is one of the most critical gases in the atmosphere.[9−11] However, continuous O_2 observations at ppm resolution are quite sparse since detecting minor O_2 variations against a large natural background is quite challenging.[12] Only a few organizations have conducted long-term atmospheric O_2 measurements, mostly in the natural background. The longest record of direct atmospheric O_2 measurements in the modern atmosphere shows a steady decline of approximately 4 ppm/yr since the late 1980s,[13] which is generally attributable to fossil fuel combustion[11] and anthropogenic modifications to the land surface including deforestation.[8,14] The aggressive urban expansion has not only substantially boosted anthropogenic fossil fuel and O_2 consumption but also deprived the ecosystem of biological O_2 production and CO_2 fixation, breaking the atmospheric O_2 balance.[15,16] A recent ice-core-based study attributed a decline in atmospheric O_2 since the Mid−Pleistocene transition (1.2−0.7 million years ago) to glacial weathering.[17] Shi et al.[18] and Chen et al.[19] measured O_2 content over the Tibetan Plateau and implied reduced hypoxia risk on the Tibetan Plateau in a warming climate.

Urban regions "inhale" O_2 from the air and 'exhale" CO_2 and atmospheric pollutants including harmful gases and fine particles. Thus, fossil fuel combustion and human respiration are two major anthropogenic O_2 sinks in the urban atmosphere. Approximately 55% of the world's population occupies only 0.37% of the global land surface.[20,21] In densely populated urban centers, human respiration could cause non-negligible perturbations in the observed O_2 and CO_2 flux and become potential sources of bias in the observation-constrained estimates since these studies ignored the influence of

Received: October 15, 2022
Revised: January 6, 2023
Accepted: January 6, 2023
Published: January 19, 2023

https://doi.org/10.1021/acs.est.2c07583
Environ. Sci. Technol. 2023, 57, 2286−2296

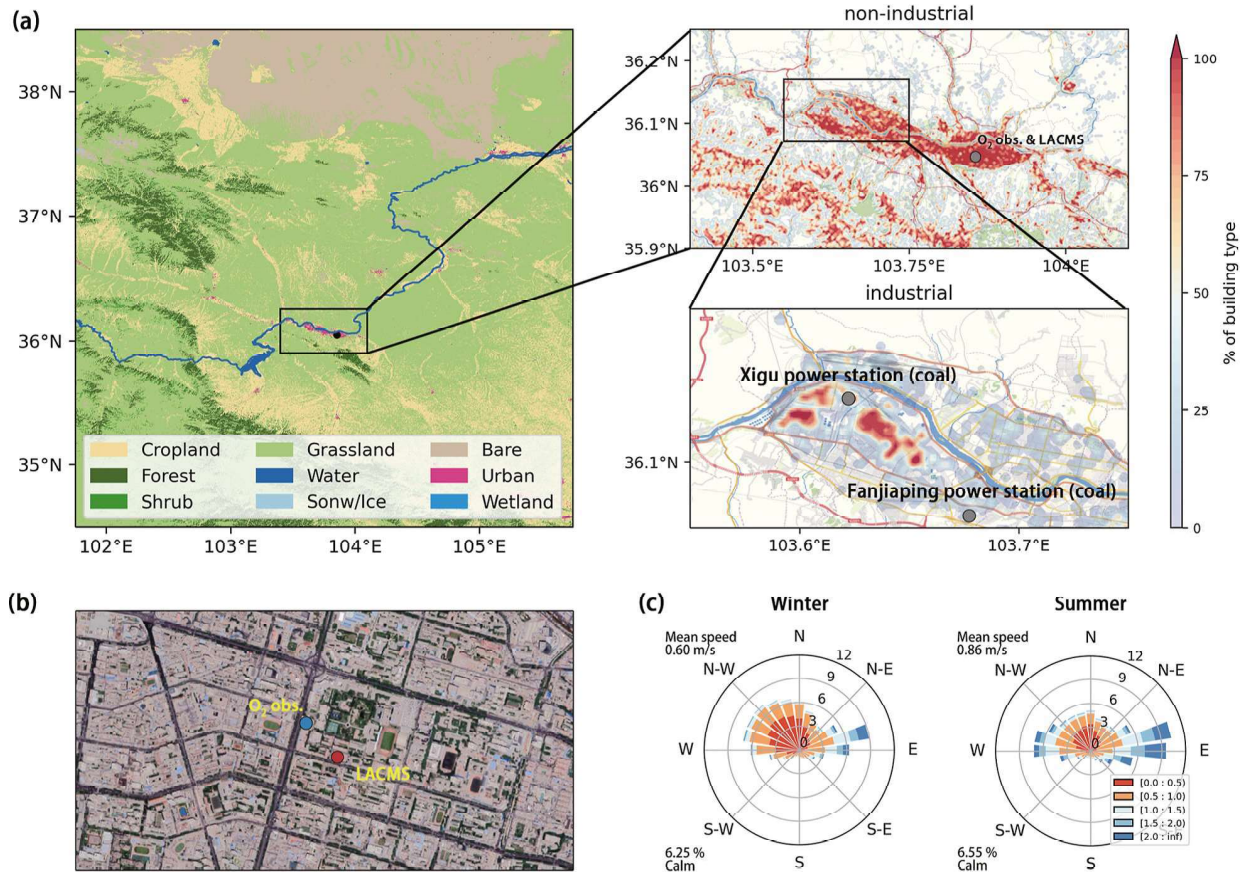

Figure 1. Geographic map and location of the observation station. (a) Map of Lanzhou Valley. The blue dot indicates the O_2 measurement site (LZU Oxygen Observatory) and the red dot indicates the LACMS. Shading indicates a population density with 0.01 × 0.01 grid spacing. (b) Satellite image around the measurement site (source: Google Earth). (c) Windrose plots at the LACMS in winter (December, January, and February) and summer (June, July, and August).

human respiration and solely attributed the observed CO_2 to fossil fuel combustion. However, only a few studies have touched upon this issue. Ciais et al.[22] estimated that respiration-related CO_2 emission reaches 30% of the fossil fuel emission for Beijing and 20% for Chongqing based on agricultural statistics. Moriwaki and Kanda[23] assumed an emission rate of 8.87 CO_2 mg s^{-1}/person, and the estimated human respiration corresponds to 17−38% of total CO_2 flux in an area with a population density of 11, 800 persons/km.[2] Another European study estimated 6.5−17% contribution to total CO_2 fluxes based on similar assumptions.[24] Cai et al.[25] estimated that human and livestock respiration can contribute to more than 5% of the carbon emission in almost half of the countries and argues that human and livestock respiration are equally crucial in the regional carbon budget. Flux measurements by Ishidoya et al.[26] quantitatively break down O_2 and CO_2 variation in urban Tokyo into combustions of liquid and gaseous fuel and estimated O_2 and CO_2 flux due to human respiration based on assumed oxidative ratio (OR) of 1.2 and population statistics. A more recent observation during the COVID-19 lockdown attributed reductions in CO_2 emission to decreased traffic volume and found a slight decrease in human respiration flux owing to decreased commuters.[27]

The above-mentioned estimates usually rely on some prior knowledge, including assumed physical activity levels for humans, ORs, food consumption and supply, and so forth, while atmospheric observations in urban regions can also be utilized to estimate the potential contribution from human respiration and fossil fuel combustion. Atmospheric pollutants, including CO, NO_x, SO_2, and so forth, could be introduced as novel constraints to quantify the anthropogenic O_2 fluxes. In previous studies, they serve as tracers for anthropogenic fossil fuel combustion due to their overlapping emission sources[28−30] since they are irrelevant to biological processes. Therefore, if atmospheric O_2 and fossil-fuel-related pollutants can be simultaneously observed, the changing relationships between O_2 and pollutants could serve as practical constraints to distinguish fossil fuel combustion from respiration in an urban atmosphere without excessive reliance on prior knowledge. Understanding these processes helps to track and measure fossil fuel combustions, validate and calibrate emission inventories, assess the efficacy of climate mitigation efforts, and provide scientific guidance for urban planning organizations.

In this work, using multiple sources of in situ observations in the urban area of Lanzhou (Figure 1), we investigated the variation in atmospheric O_2 during June 2020 to August 2021 and attempted to break down the "urban respiration" (ΔO_{2URB}) into fossil fuel combustion (ΔO_{2FF}) and human respiration (ΔO_{2RES}) under different pollution levels. We also introduced a Lagrangian atmospheric transport model (STILT)[31,32] and high-resolution urban land cover classification data sets[33] to discuss and contrast the impact of fossil fuel

https://doi.org/10.1021/acs.est.2c07583
Environ. Sci. Technol. 2023, 57, 2286−2296

combustion from industrial and nonindustrial sectors on ΔO_{2FF}.

DATA AND METHODS

Site Locations. Field measurements were conducted in Lanzhou, the capital city of Gansu Province in the semiarid region of northwestern China. Lanzhou, with a total population of >4 million, used to be one of the most polluted cities in the world, with an annual mean PM_{10} of 150 $\mu g/m^3$, according to a WHO database.[34] The city is situated in a narrow river valley surrounded by mountains (Figure 1a). The inhibited atmospheric dispersion due to the unique topography, temperature inversion, low-boundary layer height, calm wind, and scant precipitation could frequently contribute to the steady accumulation of pollutants within the valley.[35]

Urban Lanzhou can be divided into two regions according to their distinct urban functions, the downtown (nonindustrial) region and the industrial region. The industrial region (Xigu District) is located in the westernmost part of Lanzhou. As the largest petrochemical industrial base in western China, it had a large share of industrial production (50.29%) in its annual gross domestic product (GDP) in 2020.[36] Two coal-fired power stations were also located in the Xigu District. The downtown region (Chengguan District, Qilihe District, and Anning District) has the highest population density of up to 50 000 persons/km^2. The O_2 and pollutant measurements are performed in Chengguan District. The main land cover around the observation station is characterized by residential and business buildings (Figure 1b). The prevailing wind is northwest in winter and east in summer, with a high frequency of calm winds (>6.0%) throughout the year (Figure 1c). Measurements for this study were taken from July 2020 to August 2021. Since no COVID-19 lockdown was implemented in and around Lanzhou during observation, the impact of lockdown measures on observation can be ignored.

Measurements for Atmospheric Pollutants and O_2. Particulate matter (PM) concentrations (TSP, PM_{10}, $PM_{2.5}$, and PM_1), gaseous pollutants (O_3, SO_2, NO, NO_2, and CO), and meteorological parameters (temperature, relative humidity, air pressure, and wind) were observed at the Lanzhou Atmospheric Components Monitoring Superstation[35,37] (LACMS; 36.05°N, 103.87°E, Figure 1b). See Section S1 for further details about measurement instruments and methods in the LACMS station.

Air samples for O_2 measurements were collected on a building roof at Lanzhou University (approximately 300 m away from the LACMS, see Figure 1b). Online O_2 measurements were carried out using a gas chromatograph (7890B, Agilent, USA) connected with a diaphragm at a constant flow rate to prevent thermal fractionation. The air samples were separated by a Molecular Sieve 5A Plot column and detected with a thermal conductivity detector (TCD).

The interference of the dilution effect may cause significant bias when O_2 levels are reported in volume fraction units (e.g., ppm). An increase or decrease in the total air volume due to the addition or removal of other gaseous species would disturb the observed O_2 mole fraction to an extent that cannot be ignored. Thus, the concentration of atmospheric O_2 is usually reported as the relative deviation in the molar O_2/N_2 ratio from a reference value

$$\Delta(O_2/N_2) = \left[\frac{(O_2/N_2)_{sample}}{(O_2/N_2)_{reference}} - 1\right] \times 10^6$$

where the subscripts "sample" and "reference" denote the sample air and reference gas, respectively. $\Delta(O_2/N_2)$ is expressed in per meg, where 1 per meg = 1×10^{-6}. In this regard, the measured $\Delta(O_2/N_2)$ is only sensitive to the changes in O_2 and N_2 fluxes, while N_2 fluxes are typically several orders of magnitude smaller than O_2 fluxes.[13] To compare O_2 and pollutant concentrations, we report the O_2 changes in ppm units. The ratio of 4.8 per meg/ppm is used to convert the observed $\Delta(O_2/N_2)$ to the O_2 anomaly relative to an arbitrary reference concentration (ΔO_2).

The fractionation effects can cause significant bias in O_2 measurements. Fractionation effects can influence the O_2/N_2 ratio inside the measurement instrument or even at the sample intake.[38] Compared with N_2, O_2 has a higher molecular mass and tends to accumulate in areas with lower temperatures, higher pressure, and higher absolute humidity. Significant observation bias can occur when temperature, humidity, and pressure are not uniform within the instrument. In this work, we employed support vector regression to correct the original GC/TCD signals based on meteorological parameters measured during the same period (including temperature, mixing ratio, wind, pressure, etc.; see Section S2 for details). To verify our bias-corrected GC/TCD O_2 observation, a high-precision O_2 analyzer, Picarro G2207, based on the cavity ring-down spectroscopy[39] was also used for comparisons for 7 days. The high consistency between the two instruments guarantees the reliability and accuracy of the bias-corrected GC/TCD data. Comparative measurements between the gas chromatograph (7890B, Agilent, USA) and Picarro G2207 indicate a mean bias of -0.289 ± 2.908 ppm (Figure S2).

STILT Model. The stochastic time-inverted Lagrangian transport (STILT) model[39,40] is an open-source Lagrangian particle dispersion model.[31,32,40] It has been widely used to simulate the transport of pollution and greenhouse gases through the atmosphere. The STILT model releases an ensemble of air parcels from target observations (receptor) and tracks the movements of air parcels backward. The source region for the receptor is indicated by the value of footprint [ppm/(μmol m^{-2} s^{-1})]. Higher values of footprints suggest higher contributions from the source region to the receptor. The STILT model was run from Jul. 2020 to Aug. 2021 using the hourly ERA5 reanalysis data. To avoid reliance on prior emission estimation, we adopted the urban land cover data from the high-resolution World Urban Database and Access Portal Tools.[33] These data provide Local Climate Zone (LCZ) classifications at 120 m grid resolution, which shed light on localized infrastructure within the city. We convolved the simulated footprint with building type (urban buildings as well as the industrial and nonindustrial buildings within urban areas) fraction at 0.01 ° × 0.01 ° resolution, defined as the footprint-normalized urban, industrial, and nonindustrial fraction [$P_{urb}(x,y)$, $P_{ind}(x,y)$, and $P_{non\text{-}ind}(x,y)$, respectively; see Section S3.1 for details]. We then sum $P(x,y)$ across the simulated space to obtain P, which serves as a metric to quantify the urban, industrial, and nonindustrial influences (P_{urb}, P_{ind}, and $P_{non\text{-}ind}$, respectively; $P_{urb} = P_{ind} + P_{non\text{-}ind}$) on the observation site.[29] Clean (polluted) days are defined as observations with P_{urb} < 25th percentile (P_{urb} > 75th

https://doi.org/10.1021/acs.est.2c07583
Environ. Sci. Technol. 2023, 57, 2286−2296

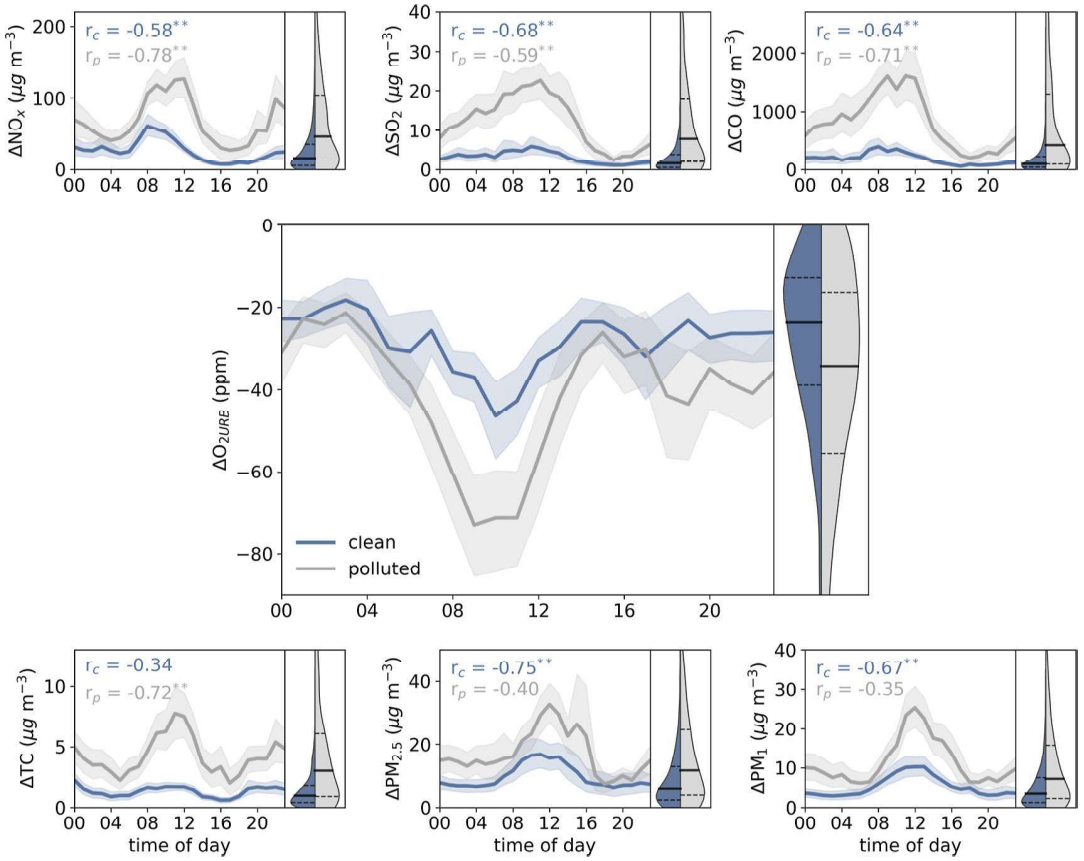

Figure 2. Averaged diurnal cycle of $\Delta Poll_i$ and ΔO_{2URB} for clean (blue) and polluted (grey) days, with shading representing a 95% confidence interval. A baseline concentration is subtracted from the original observation to highlight the anthropogenic signal. The right panel for each subplot is a violin plot that shows the probability distribution for observations under clean and polluted conditions. The Pearson correlation coefficients with the O_2 diurnal cycle on clean days (r_c) and polluted days (r_p) are shown in the left-top corner of each subplot. * and ** indicate statistical significance at the 95 and 99% confidence intervals, respectively.

percentile), indicating less (dominant) influence from urban sources.

Methods to Quantify "Urban Respiration". To focus on the anthropogenic signals of O_2 and pollutants, a "baseline condition" that signifies the background influence should be established. Here, we derived baseline concentrations of O_2 using the 99th percentile within a 24 h window centered around each hourly data point (for pollutants, the 1st percentile was selected) and then applied a 24 h running average.[30] The baseline was then subtracted from the hourly concentration to determine the enhanced anthropogenic signals in O_2 and critical pollutants (denoted by ΔO_{2URB}, ΔCO, ΔSO_2, etc.), aiming to eliminate the contribution from background biological fluxes and highlight the anthropogenic influence (human respiration and fossil fuel combustion) in downtown Lanzhou (see Section S4.1 for details). Urban lands inhale O_2 and produce CO_2 and pollutants, including CO, NO_x, SO_2, PM_1, and so forth. The following chemical reactions[28] could describe these oxidation processes

$$\text{fossil fuel} + O_2 \rightarrow H_2O + CO_2 + CO + NO_x + SO_2 + \text{other pollutants} \quad (1)$$

$$\text{carbohydrates} + O_2 \rightarrow H_2O + CO_2 \quad (2)$$

Equations 1 and 2 represent fossil fuel combustion and human respiration, respectively. The urban O_2 budget could be described as the following equation

$$\Delta O_{2URB} = \Delta O_{2FF} + \Delta O_{2RES} \quad (3)$$

where $\Delta O_{2URB} = \Delta O_2 - \Delta O_{2baseline}$.

According to the law of chemical mass balance, the O_2 consumption due to fossil fuel combustion (ΔO_{2FF}) could be parametrized as the linear combination of fossil-fuel-related pollutants

$$\Delta O_{2FF} = -\sum_{i=0}^{n} k_i \times \Delta Poll_i \quad (4)$$

where n represents the number of pollutants introduced, k_i denotes the consumption coefficient of the ith pollutant, and $Poll_i$ refers to the concentration of the ith pollutant.

To combine eqs 3 and 4, we have

$$\Delta O_{2URB} = -\sum_{i=0}^{n} k_i \times \Delta Poll_i + \Delta O_{2RES} \quad (5)$$

To solve eq 5, we bootstrapped ΔO_{2URB} and $\Delta Poll_i$ for 5000 times (each time with 30% samples). Then, non-negative least-square regression is applied to obtain 5,000 sets of bootstrap coefficients ($-k_i$) and intercepts ($-\Delta O_{2RES}$), and ΔO_{2URB} (<0) for each set is set to the absolute value ($-\Delta O_{2URB} > 0$). The averaged k_i and ΔO_{2RES} of the 5000 sets regression is obtained

https://doi.org/10.1021/acs.est.2c07583
Environ. Sci. Technol. 2023, 57, 2286−2296

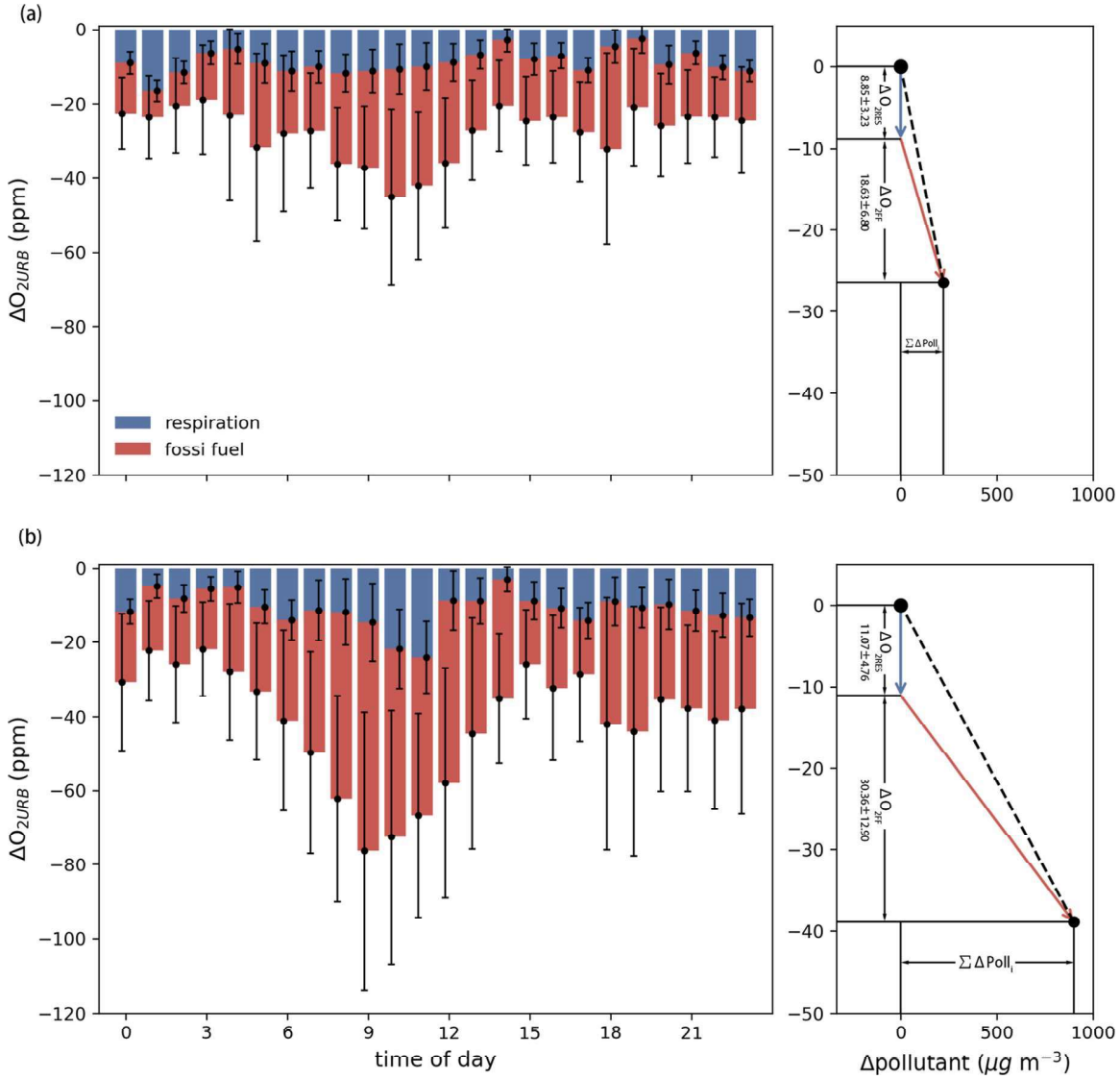

Figure 3. Contribution from respiration (blue) and fossil fuel combustion (red) to averaged hourly ΔO_{2URB} in clean (a) and polluted days (b). The right panels show the averaged changes in ΔO_{2URB} (y-axis) and Δ pollutants (x-concentration). The vectors illustrate the contribution of human respiration (blue) and fossil fuel combustion (red) related to the changes in ΔO_{2URB} (vertical axis) and Δpollutants.

for each of the 24 h in clean and polluted sets. When we estimated k_i, all the $\Delta Poll_i$ are converted to the same unit ($\mu g/m^{-3}$) and applied baseline removal. k_i (coefficient) is reported in ppm/($\mu g/m^{-3}$) and ΔO_{2RES} (intercept) is reported in ppm. We calculated $k_i \cdot \Delta Poll_i$ (ΔO_{2FF} component for each pollutant) using the observation and the derived coefficients from the bootstrap experiments to derive the contribution from each pollutant ($k_i \cdot \Delta Poll_i/\Delta O_{2FF}$, see Figures S10, S11, and 4).

It is worth noting that pollutant selection is critical since the linear combination of pollutant concentration is designed to reflect the intensity of fossil fuel combustion. If insufficient pollutants are selected for solving eq 5, ΔO_{2FF} is prone to be underfitted, leading to an overestimation of ΔO_{2RES}. Thus, optimal pollutant selections should be conducted. Here, we adopted recursive feature elimination (RFE) to select the most valuable combination of pollutants in the solution of eq 5. RFE is a widely used feature selection algorithm in machine learning models. The goal of RFE is to select valuable features by recursively considering smaller and smaller sets of features (pollutants). First, the regressor is trained on the initial set of features (pollutants) and the importance of each feature (pollutant) is obtained through regression coefficients. Then, the least important features (pollutants) are pruned from the current set of features (pollutants). That procedure is recursively repeated on the pruned set until the desired number of features (pollutants) to select is eventually reached. To find the optimal number of features, we conducted 5000 bootstraps for RFE as the number of pollutants was specified from 1 to 9. The nine pollutants initially introduced are CO, NO, NO_2, SO_2, EC (elementary carbon in $PM_{2.5}$), OC (organic carbon in $PM_{2.5}$), PM_1, $PM_{2.5}$, and PM_{10}.

RESULTS

Urban Impact on O_2 and Pollutant Levels. The ΔO_2 in the urban region displayed strong daily and seasonal cycles. The highest ΔO_2 was observed in summer, while the lowest ΔO_2 was observed in winter (see Fig S3). Both natural and anthropogenic factors contribute to O_2 fluxes into and out of

https://doi.org/10.1021/acs.est.2c07583
Environ. Sci. Technol. 2023, 57, 2286−2296

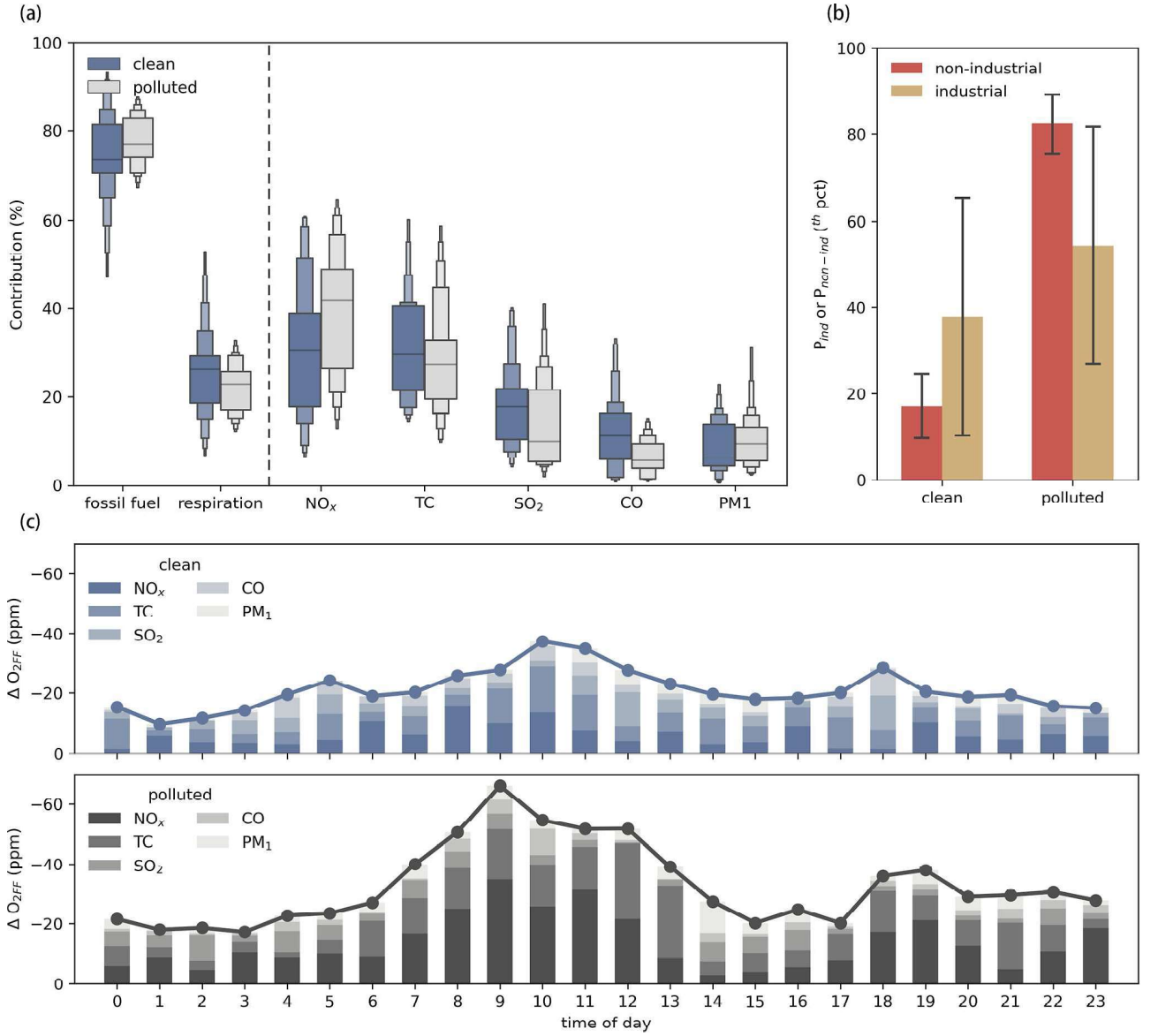

Figure 4. Contribution of potential pollutant sources to ΔO_2. (a) Daily averaged contribution from fossil-fuel-related pollutants (NO_x, TC, SO_2, CO, and PM_1) to ΔO_{2FF} on clean (blue) and polluted (grey) days. (b) Footprint percentile of industrial (orange) and nonindustrial (red) buildings under clean and polluted days. (c) Averaged diurnal cycle of ΔO_{2FF} on clean and polluted days.

the atmosphere, including variations in O_2 sources (photosynthesis) and sinks (anthropogenic O_2 consumption, etc.) and atmospheric stability that determines the dispersion and transport in the urban atmosphere. In summer, high O_2 content is mainly attributed to vegetation oxygen production and enhanced atmospheric mixing. In contrast, low ΔO_2 during winter is caused by frequent stagnant weather and surface inversion that inhibit pollutant dispersion, intensified O_2 consumption due to domestic heating, and a reduced photosynthetic effect. Due to sparse vegetation in both urban and natural landscapes in the semiarid region (Figure 1b), especially during winter, the influence of biological fluxes on ΔO_2 in Lanzhou is limited. Anthropogenic O_2 consumption and atmospheric stability seem to dominate ΔO_2 in downtown Lanzhou during the cold seasons, whereas in the warm seasons O_2 production via vegetation photosynthesis becomes apparent.

To highlight the urban impact on the anthropogenic O_2 and pollutant levels (ΔO_{2URB}, and $\Delta Poll_i$), we divided the observations into two groups: clean days and polluted days based on P_{urb}, the metric to quantify the urban influence on the observation site (see Methods). The averaged footprint and P_{urb} (x,y) for clean and polluted days are shown in Figs. S7 & S8. The averaged diurnal cycle and concentrations of ΔO_{2URB} under clean and polluted days are shown in Figure 2. The diurnal cycles of ΔO_{2URB} displayed two troughs near the morning and evening rush hours. Clean days feature higher ΔO_{2URB}, lower pollutant levels, and weaker diurnal cycle, while lower ΔO_{2URB}, higher pollutant levels, and amplified diurnal cycle are observed during polluted days. Pronounced antiphase patterns between O_2 and atmospheric pollutants are found on both clean and polluted days. High levels of O_2 are typically associated with low particulate and gaseous pollutants, implying good air quality, while declining O_2 content suggests deteriorating air quality. Robust anticorrelations between O_2

https://doi.org/10.1021/acs.est.2c07583
Environ. Sci. Technol. 2023, 57, 2286−2296

and gaseous oxides, including CO, NO_x, and SO_2, were observed throughout the year. The generation of these pollutants is associated with direct O_2 consumption as fossil fuel is combusted. Stronger ΔO_{2URB}-ΔNO_x and ΔO_{2URB}-ΔCO correlations than ΔO_{2URB}-ΔSO_2 indicate a larger contribution from transportation sectors to O_2 consumption in downtown Lanzhou,[41] while enhanced O_2−SO_2 correlation during clean days may imply intracity transport of industrial pollutants.

For fine-particulate pollutants ($PM_{2.5}$ and PM_1), stronger r_c (Pearson correlation coefficient) could be attributable to the increase in primary pollutants emitted as O_2 is consumed, while weaker r_p suggests enhanced secondary aerosol formation during the polluted episodes, which undermines the direct linkage between O_2 consumption and pollutant emissions. However, TC (EC and OC) in $PM_{2.5}$, which enters the atmosphere as both primary and secondary pollutants,[42] is shown to correlate strongly with O_2 in polluted conditions. The contrast in ΔO_{2URB}-ΔTC correlation between clean and polluted days implies a significant increase in both direct fossil-fuel-related O_2 consumption at ppm levels, and secondary formation of organic aerosol and inorganic aerosols at ppb levels as urban influence extends.

Breakdown of ΔO_{2URB} into Fossil Fuel Combustion and Human Respiration. In separating human respiration (ΔO_{2RES}) and fossil fuel combustion (ΔO_{2FF}) from the observed ΔO_{2URB} based on eq 5, the selection of pollutants is critical. Based on the RFE algorithm, optimal combinations of pollutants are picked as we gradually increase the number of pollutants introduced from 1 to 9. Figure S16a,b shows a significant improvement in fitting performance and declined ΔO_{2RES} as the number of pollutants increases. However, when more than seven pollutants are selected, no significant improvements in Pearson correlation were found and the downward trend of ΔO_{2RES} is halted. This demonstrates that the subsequent introduction of pollutants may lead to model redundancy and decrease explainability. Thus, the combination of the seven pollutants (CO, NO, NO_2, SO_2, EC, OC, and PM_1) can faithfully reproduce the O_2 decline due to fossil fuel combustion, whereas PM_{10} and $PM_{2.5}$ are excluded. The principal reason for the removal of $PM_{2.5}$ and PM_{10} is due to the relatively high contribution from both natural background emission and secondary formation in the absence of significant O_2 consumption[35,37,43] (see Section S5 for details).

Figure 3 shows the diurnal cycle of ΔO_{2RES} and ΔO_{2FF} in Lanzhou on clean and polluted days. ΔO_{2RES} displays one trough in the morning, while ΔO_{2FF} displays two troughs during morning and evening rush hours in both clean and polluted days with comparable magnitude, contrasting a weaker evening trough of ΔO_{2URB}, particularly on clean days (Figure 2). There is little difference in local emission patterns in these two scenarios, as reflected in Figure 3. However, enhanced atmospheric dispersion on clean days brings nonfossil fuel influence from outer suburbs and thus offsets and weakens local signals. The diurnal cycle of ΔO_{2RES} is similar to the flux estimation by previous observational O_2−CO_2 studies,[26,27] which is based on population statistics and assumed OR_{RES} of 1.2. Human respiration (ΔO_{2RES}) causes an 8.52 ± 3.23 ppm decline in O_2 during clean days and an 11.07 ± 4.76 ppm decline on polluted days. However, compared with clean days, $-\Delta O_{2FF}$ increased significantly from 18.63 ± 6.80 ppm (clean) to 30.36 ± 12.90 ppm (polluted). Both ΔO_{2RES} and ΔO_{2FF} display strong diurnal cycles, with a high contribution to O_2 decline during the daytime. Though both $-\Delta O_{2RES}$ and $-\Delta O_{2FF}$ increase under polluted conditions, the drops in ΔO_{2URB} are mainly attributable to fossil fuel combustion. To further determine the fossil fuel impacts of each subsector on ΔO_{2URB} and air quality warrants further breakdown of ΔO_{2FF} and explorations on the varying relationships between ΔO_{2URB} and each pollutant under different conditions.

Intracity Atmospheric Transport Revealed by Tracing ΔO_{2FF}. Figure 4a shows the averaged contribution from ΔO_{2RES} and ΔO_{2FF} to ΔO_{2URB}. During clean days, 33.08% of the ΔO_{2URB} are due to ΔO_{2RES} and 66.92% due to ΔO_{2FF}, while during polluted days, ΔO_{2RES} only account for 27.50% of the ΔO_2, and 72.50% of the ΔO_{2URB} are attributable to ΔO_{2FF}. We further attributed ΔO_{2FF} to each fossil-fuel-related pollutant (see Methods). NO_x takes the largest share of ΔO_{2FF} in both clean and polluted days, followed by TC, SO_2, CO, and PM_1. Though higher ΔO_{2URB} levels and better air quality are observed during clean days, the potential contribution from various urban sources under clean and polluted conditions differs from each other. The O_2 variation under polluted days seems to be more affected by O_2 consumption processes linked to NO_x and PM_1 emissions. For clean days, however, the influence of SO_2 and CO has grown (Figure 4b).

Weather dynamics and large-scale atmospheric motions play essential roles in determining the source and extent of atmospheric pollution.[44] There are wide discrepancies in the vertical profiles of clean and polluted days (Figure S6). For clean days, the vertical profile featured updrafts near Lanzhou and cold anomalies in the lower troposphere. The updraft around Lanzhou indicated good atmospheric ventilation, which is conducive to the dispersion and transport of pollutants and air mass. On polluted days, the vertical profile was almost the opposite of the clean days, with warm anomalies and downdrafts on the near surface. Atmospheric sounding showed surface inversion below 750 hPa (only about 600 m above the ground), which prevents vertical dispersion of pollutants and exchange of fresh clean air, traps anthropogenic pollutants in the near surface, and results in declines in atmospheric O_2 levels.

Large-scale circulation provides essential context for the transport of air pollutants at the subcity scale. Under cleaner conditions, exchanges of air between the urban region and natural background are enhanced, while it also facilitates air exchanges at smaller spatiotemporal scales between the downtown and industrial zone. The STILT simulation further indicates a higher degree of industrial influence (denoted by percentile of P_{ind}) under cleaner conditions (see Section S3.1 and Figure S8) when enhanced atmospheric dilution supports long-range transport of air mass and pollutants and diminishes pollutants from local sources. In this study, the O_2 and pollutants were measured in the downtown (nonindustrial) region, which is about 22 km away from the heavy industrial regions. Therefore, during clean days, ΔO_{2URB} variations are attributable to be influenced by both industrial and non-industrial sectors. On polluted days, local nonindustrial sectors (transportation) dominate ΔO_{2URB} concentration due to suppressed atmospheric mixing. The attribution of the diurnal cycle shows two significant peaks in NO_x-related ΔO_{2FF} during rush hours, particularly for polluted days (Figure 4c), suggesting a high contribution from traffic-related fossil fuel combustion in the downtown region. According to the MEIC inventory[45] and a recently established anthropogenic emission

https://doi.org/10.1021/acs.est.2c07583
Environ. Sci. Technol. 2023, 57, 2286−2296

inventory for Lanzhou,[46] transportation is also the largest emission source of NO_x. For clean days, weaker oscillation of the diurnal cycle and fairly even shares from different pollutant sources manifest mixed O_2 consumption from both local and remote pollutant sources. The comparisons above highlight the role of intracity atmospheric transport under a well-mixed urban atmosphere and reveal the primary O_2 consumption sector (transportation) during polluted conditions.

DISCUSSION

By integrating the findings, we propose a conceptual scheme illustrating the critical air pollution and urban O_2 consumption processes during clean and polluted days in Figure 5. The

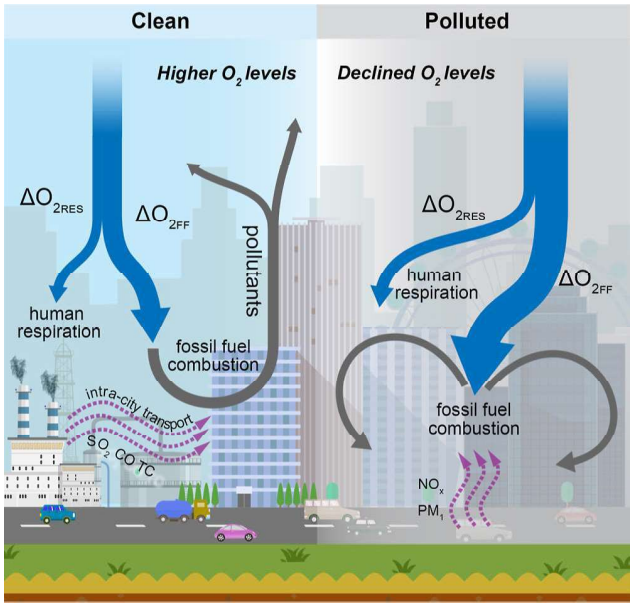

Figure 5. Conceptual scheme illustrating the critical air pollution processes during clean and polluted days. The blue arrows denote the "urban respiration" (human respiration and fossil fuel combustion). The grey arrows represent the pollutants emitted as fossil fuel is combusted, and the purple arrows indicate the intracity transport of pollutants from industrial sources (clean days) and emission enhancements from local sources (polluted days).

urban region "breathes in" atmospheric O_2 and "breath out" pollutants. Human respiration (33.08 and 27.50% for clean and polluted days, respectively) and fossil fuel combustion (66.92 and 72.50% for clean and polluted days, respectively) are major urban O_2 sinks in Lanzhou. On clean days, despite higher O_2 levels and improved air quality, good atmospheric mixing favors both diffusion and intracity transport of pollutants (SO_2, CO, and TC) from industrial sources. On polluted days, with declining atmospheric O_2 and rising pollutant levels, inhibited atmospheric dispersion traps the local pollutants within the boundary layer, and nonindustrial emissions from local sources (transportation sectors) serve as the largest O_2 sink.

The neglect of human respiration can cause underestimations of emission ratios (ER, e.g., $\Delta CO/\Delta CO_2$ and $\Delta NO_x/\Delta CO_2$) derived from direct measurements since the observed CO_2 is misattributed to fossil fuel emissions. A lot of open-air observational studies impute the higher inventory-derived ER to overestimation by emission inventories,[29,30,47] while excellent agreements between local inventory CO/CO_2 ratio for the traffic sector and the observed $\Delta CO/\Delta CO_2$ ratio are obtained in a tunnel study, in which CO_2 and pollutants (CO, NO_x, and VOCs) measurements were performed in a road tunnel in Paris,[48] which is close to the origin of the air mass. It is worth stressing that the neglect of human respiration may not necessarily indicate that ERs from previous observations are incorrect, and bias may also occur in ERs derived from inventory. The observed ERs in the Paris study,[48] which is conducted in a tunnel close to the major emission sources, may be less influenced by human respiration. To mitigate the impact of human respiration on the observed ERs, we suggest that necessary adjustments are needed in the selection of observatory location (e.g., away from densely populated regions) and/or postprocessing of the observed CO_2 (e.g., subtraction of respiration-related component from the observed CO_2 variability). In addition, accurate estimation of the CO_2 and O_2 fluxes due to human respiration, especially for densely populated regions, could be important for constraining urban carbon budgets and the establishment of regional emission inventories.

The varying relationships between O_2 and pollutants under different conditions unfold the dynamics of urban respiration and provide insights into the anthropogenic O_2 and energy consumption, pollutant emission, and intracity atmospheric transport processes. This study is one of the first to break down urban O_2 variability based on simultaneous O_2 and pollutant measurements. It is worth noting that the conclusion should be interpreted with caution due to the following limitations of the study. Although an optimal combination of pollutants determined by the RFE algorithm is introduced to the linear model and variance inflation factor analysis has revealed a weak impact from multicollinearity (see Figure S20), the framework proposed in this study may not be able to fully capture the complex chemical transformations in the urban atmosphere (i.e., secondary generation of organic and inorganic aerosols including nitrate, sulfate, and ammonium). In addition, despite the removal of the baseline determined by the 99th (and 1st) percentile, the impact of biological flux on ΔO_{2URB} is not yet quantified. By inspecting the simulation bias, we found a larger negative bias (~1 ppm) in the afternoon and summertime when an enhanced effect of photosynthesis is observed (see Section S4.3). Nevertheless, it should be noted that the model bias could also be caused by other unknown sources. The lack of consideration for vegetation could be a potential bias that deserves further consideration for future studies.

Simultaneous measurements of O_2, CO_2, and fossil-fuel-related atmospheric pollutants are necessary. They can constrain the ORs for human respiration and fossil fuel combustion, providing additional constraints for regional and global carbon budgets as well as multiscale emission inventories. A similar research framework could be applied to a wider spatial domain to trace anthropogenic emission, energy, and O_2 consumption as well as calibrate emission inventories using multiple sources of observations including satellite retrievals,[49] urban mobile observations,[50,51] and so forth. In addition, the nonlinear relationships among O_2, CO_2, and species with short lifetimes could be explored using nonlinear models, for example, the AI models including random forests regressor, deep neural networks, and so forth.

https://doi.org/10.1021/acs.est.2c07583
Environ. Sci. Technol. 2023, 57, 2286−2296

■ ASSOCIATED CONTENT

Supporting Information

The Supporting Information is available free of charge at https://pubs.acs.org/doi/10.1021/acs.est.2c07583.

Pollution measurements at the LACMS station; instrument bias correction for O_2 measurements; classification of clean and polluted days; background signal removal; and critical pollutants selection for ΔO_{2URB} breakdown (PDF)

■ AUTHOR INFORMATION

Corresponding Author

Jianping Huang − *Collaborative Innovation Center for Western Ecological Safety, Lanzhou University, Lanzhou 730000, China; Land-atmosphere Interaction and Its Climatic Effects Group, State Key Laboratory of Tibetan Plateau Earth System, Resources and Environment (TPESRE), Institute of Tibetan Plateau Research, Beijing 100101, China;* orcid.org/0000-0003-2845-797X; Email: hjp@lzu.edu.cn

Authors

Xiaoyue Liu − *Key Laboratory for Semi-Arid Climate Change of the Ministry of Education, College of Atmospheric Sciences, Lanzhou University, Lanzhou 730000, China;* orcid.org/0000-0001-8074-3362

Li Wang − *Collaborative Innovation Center for Western Ecological Safety, Lanzhou University, Lanzhou 730000, China*

Xinbo Lian − *Key Laboratory for Semi-Arid Climate Change of the Ministry of Education, College of Atmospheric Sciences, Lanzhou University, Lanzhou 730000, China*

Changyu Li − *Key Laboratory for Semi-Arid Climate Change of the Ministry of Education, College of Atmospheric Sciences, Lanzhou University, Lanzhou 730000, China*

Lei Ding − *Key Laboratory for Semi-Arid Climate Change of the Ministry of Education, College of Atmospheric Sciences, Lanzhou University, Lanzhou 730000, China*

Yun Wei − *Department of Atmospheric Science, School of Environmental Studies, China University of Geosciences, Wuhan 430074, China*

Siyu Chen − *Key Laboratory for Semi-Arid Climate Change of the Ministry of Education, College of Atmospheric Sciences, Lanzhou University, Lanzhou 730000, China;* orcid.org/0000-0003-2532-6050

Yongqi Wang − *Key Laboratory for Semi-Arid Climate Change of the Ministry of Education, College of Atmospheric Sciences, Lanzhou University, Lanzhou 730000, China*

Shixue Li − *Graduate School of Environmental Science, Hokkaido University, Sapporo 060-0810, Japan*

Jinsen Shi − *Collaborative Innovation Center for Western Ecological Safety, Lanzhou University, Lanzhou 730000, China*

Complete contact information is available at: https://pubs.acs.org/10.1021/acs.est.2c07583

Author Contributions

X.L. and J.H. designed the study and contributed to the ideas, data analysis, and manuscript writing. L.W. and X.L. contributed to the data processing, interpretation, and manuscript writing. All of the authors contributed to the discussion and interpretation of the manuscript. All of the authors reviewed the manuscript.

Notes

The authors declare no competing financial interest.

■ ACKNOWLEDGMENTS

This work was jointly supported by the National Science Foundation of China (41991231 and 91937302), the Second Tibetan Plateau Scientific Expedition and Research Program (STEP), grant no. 2019QZKK0602, the Youth Science and Technology Fund Project of Gansu Province of China (21JR7RA528), and the Fundamental Research Funds for the Central Universities (lzujbky-2021-64).

■ REFERENCES

(1) United Nations Population Division. World Urbanization Prospects: The 2018 Revision, 2018. https://population.un.org/wup/Publications/Files/WUP2018-Report.pdf (accessed Dec 25, 2022).

(2) Churkina, G.The Role of Urbanization in the Global Carbon Cycle. *Front. Ecol. Evol.***2016**, *3*. DOI: 10.3389/fevo.2015.00144.

(3) Wang, J.; Feng, J.; Yan, Z.; Chen, Y. Future Risks of Unprecedented Compound Heat Waves Over Three Vast Urban Agglomerations in China. *Earths Future* **2020**, *8*, No. e2020EF001716.

(4) Huang, J.; Li, Y.; Fu, C.; Chen, F.; Fu, Q.; Dai, A.; Shinoda, M.; Ma, Z.; Guo, W.; Li, Z.; Zhang, L.; Liu, Y.; Yu, H.; He, Y.; Xie, Y.; Guan, X.; Ji, M.; Lin, L.; Wang, S.; Yan, H.; Wang, G. Dryland Climate Change: Recent Progress and Challenges. *Rev. Geophys.* **2017**, *55*, 719−778.

(5) Liang, D.; Shi, L.; Zhao, J.; Liu, P.; Sarnat, J. A.; Gao, S.; Schwartz, J.; Liu, Y.; Ebelt, S. T.; Scovronick, N.; Chang, H. H. Urban Air Pollution May Enhance COVID-19 Case-Fatality and Mortality Rates in the United States. *Innovation* **2020**, *1*, 100047.

(6) Guo, W.; Chen, B.; Li, G.; Liu, M.; Liu, X.; Chen, Q.; Zhang, X.; Li, S.; Chen, S.; Feng, W.; Zhang, R.; Chen, M.; Shi, T. Ambient PM2.5 and Related Health Impacts of Spontaneous Combustion of Coal and Coal Gangue. *Environ. Sci. Technol.* **2021**, *55*, 5763−5771.

(7) Chen, S.; Zhang, X.; Lin, J.; Huang, J.; Zhao, D.; Yuan, T.; Huang, K.; Luo, Y.; Jia, Z.; Zang, Z.; Qiu, Y.; Xie, L. Fugitive Road Dust PM2.5 Emissions and Their Potential Health Impacts. *Environ. Sci. Technol.* **2019**, *53*, 8455−8465.

(8) Wei, Y.; Wu, J.; Huang, J.; Liu, X.; Han, D.; An, L.; Yu, H.; Huang, J. Declining Oxygen Level as an Emerging Concern to Global Cities. *Environ. Sci. Technol.* **2021**, *55*, 7808−7817.

(9) Li, C.; Huang, J.; Ding, L.; Liu, X.; Yu, H.; Huang, J. Increasing Escape of Oxygen From Oceans Under Climate Change. *Geophys. Res. Lett.* **2020**, *47*, No. e2019GL086345.

(10) Huang, J.; Liu, X.; He, Y.; Shen, S.; Hou, Z.; Li, S.; Li, C.; Yao, L.; Huang, J. The Oxygen Cycle and a Habitable Earth. *Sci. China Earth Sci.* **2021**, *64*, 511−528.

(11) Liu, X.; Huang, J.; Huang, J.; Li, C.; Ding, L.; Meng, W. Estimation of Gridded Atmospheric Oxygen Consumption from 1975 to 2018. *J. Meteorol. Res.* **2020**, *34*, 646−658.

(12) Keeling, R. F.; Manning, A. C.*Studies of Recent Changes in Atmospheric O2 Content*, 2nd ed.; Elsevier Ltd., 2014; Vol. 5. DOI: 10.1016/B978-0-08-095975-7.00420-4.,

(13) Keeling, R. F.*Development of an Interferometric Oxygen Analyzer for Precise Measurement of the Atmospheric O2 Mole Fraction*; Harvard University: Cambridge, 1988.

(14) Huang, J.; Huang, J.; Liu, X.; Li, C.; Ding, L.; Yu, H. The Global Oxygen Budget and Its Future Projection. *Sci. Bull.* **2018**, *63*, 1180−1186.

(15) Han, D.; Huang, J.; Ding, L.; Liu, X.; Li, C.; Yang, F. Oxygen Footprint: An Indicator of the Anthropogenic Ecosystem Changes. *Catena* **2021**, *206*, 105501.

(16) Han, D.; Huang, J.; Ding, L.; Zhang, G.; Liu, X.; Li, C.; Yang, F. Breaking the Ecosystem Balance Over the Tibetan Plateau. *Earths Future* **2022**, *10*, No. e2022EF002890.
(17) Yan, Y.; Brook, E. J.; Kurbatov, A. v.; Severinghaus, J. P.; Higgins, J. A. Ice Core Evidence for Atmospheric Oxygen Decline since the Mid-Pleistocene Transition. *Sci. Adv.* **2021**, *7*, No. eabj9341.
(18) Shi, P.; Chen, Y.; Zhang, G.; Tang, H.; Chen, Z.; Yu, D.; Yang, J.; Ye, T.; Wang, J.; Liang, S.; Ma, Y.; Wu, J.; Gong, P. Factors contributing to spatial-temporal variations of observed oxygen concentration over the Qinghai-Tibetan Plateau. *Sci. Rep.* **2021**, *11*, 17338.
(19) Chen, Y.; Zhang, G.; Chen, Z.; Yang, X.; Chen, B.; Ma, Y.; Xie, H.; Luo, Q.; Yang, J.; Ye, T.; Yu, D.; Wang, J.; Tang, H.; Chen, Z.; Shi, P. A Warming Climate May Reduce Health Risks of Hypoxia on the Qinghai-Tibet Plateau. *Sci. Bull.* **2022**, *67*, 341−344.
(20) Cai, Q.; Zeng, N.; Zhao, F.; Han, P.; Liu, D.; Lin, X.; Chen, J. The Impact of Human and Livestock Respiration on CO2 Emissions from 14 Global Cities. *Carbon Bal. Manag.* **2022**, *17*, 11−12.
(21) Klein Goldewijk, K. K.; Beusen, A.; Doelman, J.; Stehfest, E. Anthropogenic Land Use Estimates for the Holocene - HYDE 3.2. *Earth Syst. Sci. Data* **2017**, *9*, 927−953.
(22) Ciais, P.; Bousquet, P.; Freibauer, A.; Naegler, T. Horizontal Displacement of Carbon Associated with Agriculture and Its Impacts on Atmospheric CO2. *Global Biogeochem. Cycles* **2007**, *21*, a.
(23) Moriwaki, R.; Kanda, M. Seasonal and Diurnal Fluxes of Radiation, Heat, Water Vapor, and Carbon Dioxide over a Suburban Area. *J. Appl. Meteorol. Climatol.* **2004**, *43*, 1700−1710.
(24) Goret, M.; Masson, V.; Schoetter, R.; Moine, M. P. Inclusion of CO2 Flux Modelling in an Urban Canopy Layer Model and an Evaluation over an Old European City Centre. *Atmos. Environ.: X* **2019**, *3*, 100042.
(25) Cai, Q.; Yan, X.; Li, Y.; Wang, L. Global Patterns of Human and Livestock Respiration. *Sci. Rep.* **2018**, *8*, 3−6.
(26) Ishidoya, S.; Sugawara, H.; Terao, Y.; Kaneyasu, N.; Aoki, N.; Tsuboi, K.; Kondo, H. L. O_2 : CO_2 exchange ratio for net turbulent flux observed in an urban area of Tokyo, Japan, and its application to an evaluation of anthropogenic CO_2 emissions. *Atmos. Chem. Phys.* **2020**, *20*, 5293−5308.
(27) Sugawara, H.; Ishidoya, S.; Terao, Y.; Takane, Y.; Kikegawa, Y.; Nakajima, K. Anthropogenic CO 2 Emissions Changes in an Urban Area of Tokyo, Japan, Due to the COVID-19 Pandemic: A Case Study During the State of Emergency in April-May 2020. *Geophys. Res. Lett.* **2021**, *48*, 1−10.
(28) Steinbach, J.; Gerbig, C.; Rödenbeck, C.; Karstens, U.; Minejima, C.; Mukai, H.; Rödenbeck, C.; Karstens, U.; Minejima, C.; Mukai, H. The CO_2 release and Oxygen uptake from Fossil Fuel Emission Estimate (COFFEE) dataset: effects from varying oxidative ratios. *Atmos. Chem. Phys.* **2011**, *11*, 6855−6870.
(29) Wu, D.; Liu, J.; Wennberg, P. O.; Palmer, P. I.; Nelson, R. R.; Kiel, M.; Eldering, A. Towards Sector-Based Attribution Using Intra-city Variations in Satellite-Based Emission Ratios between CO 2 and CO. *Atmos. Chem. Phys.* **2022**, *22*, 14547−14570.
(30) Bares, R.; Lin, J. C.; Hoch, S. W.; Baasandorj, M.; Mendoza, D. L.; Fasoli, B.; Mitchell, L.; Catharine, D.; Stephens, B. B. The Wintertime Covariation of CO 2 and Criteria Pollutants in an Urban Valley of the Western United States. *J. Geophys. Res.: Atmos.* **2018**, *123*, 2684−2703.
(31) Wu, D.; Lin, J.; Fasoli, B.; Oda, T.; Ye, X.; Lauvaux, T.; Yang, E.; Kort, E. A Lagrangian approach towards extracting signals of urban CO_2 emissions from satellite observations of atmospheric column CO_2 (XCO_2): X-Stochastic Time-Inverted Lagrangian Transport model ("X-STILT v1"). *Geosci. Model Dev.* **2018**, *11*, 4843−4871.
(32) Fasoli, B.; Lin, J. C.; Bowling, D. R.; Mitchell, L.; Mendoza, D. Simulating atmospheric tracer concentrations for spatially distributed receptors: updates to the Stochastic Time-Inverted Lagrangian Transport model's R interface (STILT-R version 2). *Geosci. Model Dev.* **2018**, *11*, 2813−2824.
(33) Ching, J.; Mills, G.; Bechtel, B.; See, L.; Feddema, J.; Wang, X.; Ren, C.; Brousse, O.; Martilli, A.; Neophytou, M.; Mouzourides, P.; Stewart, I.; Hanna, A.; Ng, E.; Foley, M.; Alexander, P.; Aliaga, D.; Niyogi, D.; Shreevastava, A.; Bhalachandran, P.; Masson, V.; Hidalgo, J.; Fung, J.; Andrade, M.; Baklanov, A.; Dai, W.; Milcinski, G.; Demuzere, M.; Brunsell, N.; Pesaresi, M.; Miao, S.; Mu, Q.; Chen, F.; Theeuwes, N. WUDAPT: An Urban Weather, Climate, and Environmental Modeling Infrastructure for the Anthropocene. *Bull. Am. Meteorol. Soc.* **2018**, *99*, 1907−1924.
(34) World Health Organization (WHO). Air quality database: Update, 2011. https://www.who.int/data/gho/data/themes/air-pollution/who-air-quality-database/2011 (accessed Dec 25, 2022) .
(35) Du, T.; Wang, M.; Guan, X.; Zhang, M.; Zeng, H.; Chang, Y.; Zhang, L.; Tian, P.; Shi, J.; Tang, C. Characteristics and Formation Mechanisms of Winter Particulate Pollution in Lanzhou, Northwest China. *J. Geophys. Res.: Atmos.* **2020**, *125*, 1−17.
(36) Lanzhou Municipal Bureau of Statistics; Lanzhou Investigation Team (National Bureau of Statistics). *Lanzhou Statistical Yearbook 2020*; China Statistics Press, 2020.
(37) Wang, M.; Tian, P.; Wang, L.; Yu, Z.; Du, T.; Chen, Q.; Guan, X.; Guo, Y.; Zhang, M.; Tang, C.; Chang, Y.; Shi, J.; Liang, J.; Cao, X.; Zhang, L. High contribution of vehicle emissions to fine particulate pollutions in Lanzhou, Northwest China based on high-resolution online data source appointment. *Sci. Total Environ.* **2021**, *798*, 149310.
(38) Steinbach, J.*Enhancing the Usability of Atmospheric Oxygen Measurements through Emission Source Characterization and Airborne Measurements*; Friedrich Schiller University, 2010.
(39) Berhanu, T. A.; Hoffnagle, J.; Rella, C.; Kimhak, D.; Nyfeler, P.; Leuenberger, M. High-Precision Atmospheric Oxygen Measurement Comparisons between a Newly Built CRDS Analyzer and Existing Measurement Techniques. *Atmos. Meas. Tech.* **2019**, *12*, 6803−6826.
(40) Lin, J. C. A. A near-field tool for simulating the upstream influence of atmospheric observations: The Stochastic Time-Inverted Lagrangian Transport (STILT) model. *J. Geophys. Res.* **2003**, *108*, ACH 2-1−ACH 2-17, DOI: 10.1029/2002JD003161.
(41) Reşitoğlu, İ. A.; Altinişik, K.; Keskin, A. The Pollutant Emissions from Diesel-Engine Vehicles and Exhaust Aftertreatment Systems. *Clean Technol. Environ. Policy* **2015**, *17*, 15−27.
(42) Szidat, S.; Ruff, M.; Perron, N.; Wacker, L.; Synal, H.-A.; Hallquist, M.; Shannigrahi, A. S.; Yttri, K. E.; Dye, C.; Simpson, D. Fossil and non-fossil sources of organic carbon (OC) and elemental carbon (EC) in Göteborg, Sweden. *Atmos. Chem. Phys.* **2009**, *9*, 1521−1535.
(43) Guan, X.; Wang, M.; Du, T.; Tian, P.; Zhang, N.; Shi, J.; Chang, Y.; Zhang, L.; Zhang, M.; Song, X.; Sun, Y. Wintertime Aerosol Optical Properties in Lanzhou, Northwest China: Emphasis on the Rapid Increase of Aerosol Absorption under High Particulate Pollution. *Atmos. Environ.* **2021**, *246*, 118081.
(44) Cai, W.; Li, K.; Liao, H.; Wang, H.; Wu, L. Weather Conditions Conducive to Beijing Severe Haze More Frequent under Climate Change. *Nat. Clim. Change* **2017**, *7*, 257−262.
(45) Li, M.; Liu, H.; Geng, G.; Hong, C.; Liu, F.; Song, Y.; Tong, D.; Zheng, B.; Cui, H.; Man, H.; Zhang, Q.; He, K. Anthropogenic Emission Inventories in China: A Review. *Natl. Sci. Rev.* **2017**, *4*, 834−866.
(46) Guo, W.; Li, G.; Chen, B.; Xia, J.; Zhang, R.; Liu, X.; Zhu, Y.; Chen, Q. Establishment of a High-Resolution Anthropogenic Emission Inventory and Its Evaluation Using the WRF-Chem Model for Lanzhou. *Environ. Sci.* **2021**, *42*, 634−642.
(47) Che, K.; Liu, Y.; Cai, Z.; Yang, D.; Wang, H.; Ji, D.; Yang, Y.; Wang, P. Characterization of Regional Combustion Efficiency using ΔXCO: ΔXCO2 Observed by a Portable Fourier-Transform Spectrometer at an Urban Site in Beijing. *Adv. Atmos. Sci.* **2022**, *39*, 1299−1315.
(48) Ammoura, L.; Xueref-Remy, I.; Gros, V.; Baudic, A.; Bonsang, B.; Petit, J.-E.; Perrussel, O.; Bonnaire, N.; Sciare, J.; Chevallier, F. Atmospheric measurements of ratios between CO_2 and co-emitted species from traffic: a tunnel study in the Paris megacity. *Atmos. Chem. Phys.* **2014**, *14*, 12871−12882.

(49) Reuter, M.; Buchwitz, M.; Hilboll, A.; Richter, A.; Schneising, O.; Hilker, M.; Heymann, J.; Bovensmann, H.; Burrows, J. P. Decreasing Emissions of NOx Relative to CO2 in East Asia Inferred from Satellite Observations. *Nat. Geosci.* **2014**, *7*, 792−795.
(50) Mitchell, L. E.; Crosman, E. T.; Jacques, A. A.; Fasoli, B.; Leclair-Marzolf, L.; Horel, J.; Bowling, D. R.; Ehleringer, J. R.; Lin, J. C. Monitoring of Greenhouse Gases and Pollutants across an Urban Area Using a Light-Rail Public Transit Platform. *Atmos. Environ.* **2018**, *187*, 9−23.
(51) Mallia, D. v.; Mitchell, L. E.; Kunik, L.; Fasoli, B.; Bares, R.; Gurney, K. R.; Mendoza, D. L.; Lin, J. C. Constraining Urban CO2 Emissions Using Mobile Observations from a Light Rail Public Transit Platform. *Environ. Sci. Technol.* **2020**, *54*, 15613−15621.

https://doi.org/10.1021/acs.est.2c07583
Environ. Sci. Technol. 2023, 57, 2286−2296